Geometric control of vascular networks to enhance engineered tissue integration and function

Jan D. Baranski[a,1], Ritika R. Chaturvedi[a,1], Kelly R. Stevens[b,1], Jeroen Eyckmans[a], Brian Carvalho[b], Ricardo D. Solorzano[a], Michael T. Yang[a], Jordan S. Miller[a], Sangeeta N. Bhatia[b,c,d,e,f], and Christopher S. Chen[a,2]

[a]Department of Bioengineering, School of Engineering and Applied Science, University of Pennsylvania, Philadelphia, PA 19104; [b]Harvard-MIT Health Sciences and Technology, Institute for Medical Engineering and Science, Massachusetts Institute of Technology, Cambridge, MA 02139 [c]Howard Hughes Medical Institute, Cambridge, MA 02139; [d]Department of Electrical Engineering and Computer Science, Massachusetts Institute of Technology, Cambridge, MA 02139; [e]David H. Koch Institute for Integrative Cancer Research, Massachusetts Institute of Technology, Cambridge, MA 02139; and [f]Department of Medicine, Brigham and Women's Hospital, Harvard Medical School, Boston, MA 02115

Edited by Michael A. Gimbrone, Brigham and Women's Hospital, Harvard Medical School, Boston, MA, and approved March 27, 2013 (received for review October 16, 2012)

Tissue vascularization and integration with host circulation remains a key barrier to the translation of engineered tissues into clinically relevant therapies. Here, we used a microtissue molding approach to demonstrate that constructs containing highly aligned "cords" of endothelial cells triggered the formation of new capillaries along the length of the patterned cords. These vessels became perfused with host blood as early as 3 d post implantation and became progressively more mature through 28 d. Immunohistochemical analysis showed that the neovessels were composed of human and mouse endothelial cells and exhibited a mature phenotype, as indicated by the presence of alpha-smooth muscle actin–positive pericytes. Implantation of cords with a prescribed geometry demonstrated that they provided a template that defined the neovascular architecture in vivo. To explore the utility of this geometric control, we implanted primary rat and human hepatocyte constructs containing randomly organized endothelial networks vs. ordered cords. We found substantially enhanced hepatic survival and function in the constructs containing ordered cords following transplantation in mice. These findings demonstrate the importance of multicellular architecture in tissue integration and function, and our approach provides a unique strategy to engineer vascular architecture.

tissue engineering | regenerative medicine | angiogenesis | vascular biology | liver

Engineered tissues are emerging as a viable approach to address the scarce supply of heterologous donor organs available for transplantation (1). However, the field has not yet identified an effective strategy to vascularize such tissue constructs, thus limiting current successes primarily to thin, avascular tissues (2). In vascularized tissues, it is estimated that cells must be located within 150–200 μm of the nearest capillary to survive and function optimally (3), although this distance may vary depending on the metabolic demands of different cell types. Although some tissues can function with lower capillary densities, adequate perfusion of metabolically active tissue requires intimate localization of parenchymal cells to a dense vasculature in a highly organized manner (1, 4, 5). For example, the liver has a precisely defined organization in which hepatocytes and microvessels are interdigitated in a highly aligned microarchitecture (2, 6). In addition, the architecture of the vasculature itself—the branching frequency and angles, alignment of vessels, and tortuosity—constrains gradients of metabolite exchange and the overall flow fields through the tissue. Engineering such tissues therefore will require approaches to define the geometric architecture of vascular networks for tissue-specific applications.

Although several strategies have been explored to enhance tissue vascularization, including immobilization or controlled release of proangiogenic factors (3, 7, 8), studies in which the tissue is seeded with exogenous endothelial and mural cells before implantation have been particularly promising (9–12). Recent progress suggests that allowing vascular cells to form rudimentary vascular networks either in vitro ("prevascularization"), or in vivo, results in enhanced integration of grafted endothelial cells (ECs) with host vasculature and parenchymal cell survival following implantation (12–16). Although these strategies demonstrate potential, they rely on the spontaneous self-organization of randomly seeded cells and leave open the question as to whether more directed control over network formation might allow further improvement to their function.

Here, we report the development of a unique approach for rapidly creating spatially organized vascular architectures within engineered tissues in vivo. Our approach uses micropatterning techniques to organize ECs into geometrically defined "cords," which in turn act as a template after implantation for the guided formation of patterned capillaries integrated with host tissue. We demonstrate that spatial patterning of vascular architecture within engineered hepatic tissues leads to significantly increased levels of albumin activity, a marker of differentiated hepatocyte function, for at least 3 wk in vivo compared with nonpatterned controls. These findings demonstrate that geometric control of vascular architecture modulates the function of engineered tissues and therefore has broad application in the translation of cell-based regenerative therapies.

Results

Patterned Assemblies of EC Cords Induces a Vascular Response. Adapting a previously developed approach (1, 17), geometrically defined cords of ECs that encase a collagen core were generated by seeding a suspension of human umbilical vein ECs (HUVECs) and mouse mesenchymal cells (C3H10T1/2) in liquid type I collagen into 150-μm–wide microchannels by centrifugation (Fig. 1*A*). After the collagen was polymerized and upon culture, the cells rapidly self-assembled into cords over approximately 4 h, during which they contracted to roughly 50% of their original diameter (Fig. 1*B*). This cord contraction was driven by myosin-mediated contractile activity, as cells treated with a nonmuscle myosin inhibitor (blebbistatin) or a Rho-associated protein kinase (ROCK) inhibitor (Y27632) immediately after seeding failed to form cords (Fig. S1). Time-lapse imaging of fluorescently labeled cells showed that the small

Author contributions: J.D.B., R.R.C., K.R.S., S.N.B., and C.S.C. designed research; J.D.B., R.R.C., K.R.S., J.E., B.C., R.D.S., and M.T.Y. performed research; J.D.B., R.R.C., K.R.S., and J.S.M. contributed new reagents/analytic tools; J.D.B., R.R.C., K.R.S., J.E., B.C., and R.D.S. analyzed data; and J.D.B., R.R.C., K.R.S., S.N.B., and C.S.C. wrote the paper.

The authors declare no conflict of interest.

This article is a PNAS Direct Submission.

[1]J.D.B., R.R.C, and K.R.S. contributed equally to this work.

[2]To whom correspondence should be addressed. E-mail: chrischen@seas.upenn.edu.

This article contains supporting information online at www.pnas.org/lookup/suppl/doi:10.1073/pnas.1217796110/-/DCSupplemental.

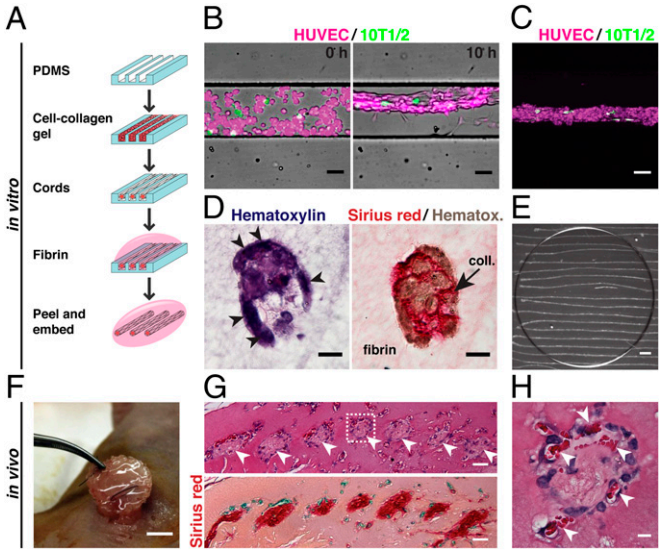

Fig. 1. Generation of EC cords. (*A*) Schematic representation of the process used to generate cords. Collagen, red; fibrin, pink. (*B*) Merged phase and fluorescence images of cord formation at 0 and 10 h within PDMS microchannels (HUVECs, calcein AM red-orange; 10T1/2s, calcein AM green; bar, 50 μm). (*C*) Maximum-intensity z-projection of fluorescently labeled HUVECs (magenta) and 10T1/2s (green) (bar, 50 μm). (*D*) H&E and Sirius red/hematoxylin staining of paraffin-embedded cord constructs showing distribution of cells and collagen in cross-section (bar, 20 μm). (*E*) Bright field micrograph of EC cord constructs after removal from PDMS substrate and embedding within fibrin gel. Dark circle indicates the portion of the gel that was cut with a biopsy punch in preparation for implantation (bar, 500 μm). (*F*) Tissue construct containing cords sutured in place adjacent to the parametrial fat pad of an athymic mouse. (*G*) H&E and Sirius red staining of cord-containing tissue constructs resected after 7 d in vivo. Arrowheads indicate the location of cords (bar, 25 μm). (*H*) Inset showing higher magnification H&E staining of single cord. Arrowheads indicate areas of blood around the periphery of the cord (bar, 5 μm).

population of 10T1/2s remained randomly distributed along the length of the primarily HUVEC cords throughout the contraction process (Fig. 1 *B* and *C*). Hematoxylin and eosin (H&E) and Sirius red staining of cross-sections of the fully formed, paraffin-embedded cords demonstrated clustering and wrapping of cells around a core of compacted collagen (Fig. 1*D*).

To test the ability of patterned EC cords to induce vascularization in vivo, we removed the cords from the polydimethylsiloxane (PDMS) backing by first polymerizing a layer of fibrin over the top of the substrate, peeling the PDMS away to leave the cords on the surface of the fibrin layer, and then polymerizing a second layer of fibrin to fully encase the cords (Fig. 1 *A* and *E*). Following assembly, the constructs were sutured directly to the parametrial fat pad in the intraperitoneal (i.p.) space of athymic mice (Fig. 1*F*) and resected after 7 d. Histological staining of the paraffin-embedded tissues demonstrated the presence of collagen-rich, cell-laden structures within the fibrin implant that were organized spatially in a pattern mimicking the original position of the implanted cords (Fig. 1*G*). Higher magnification of these remnant cords indicated the presence of blood in the cell-rich regions around the perimeter alongside the axis of the cords, suggesting a directed vascularization response (Fig. 1*H*).

Recapitulation of Rudimentary Vessel Maturation Occurs Along Implanted Cords to Result in New Capillaries. To further characterize the blood vessel formation process resulting from the implantation of cords, we harvested tissue constructs at days 3, 5, 7, 14, and 28 post implantation (PI) (*SI Materials and Methods*). H&E staining of resected tissues suggested the presence of red blood cells (RBCs) around the perimeter of cords as early as 3 d PI (Fig. 2*A*). Large areas of blood were present at 3 and 5 d PI and were surrounded by a fragmented layer of cells, reminiscent of the pattern observed in leaky vasculature. Loose cellular structures were replaced over time by a smaller, more definitive vessel-like cellular lining stereotypical of mature microvessels that persisted at least out to 28 d PI. Sirius red/fast green staining demonstrated the presence of collagen within the cords throughout the entire time course (Fig. 2*B*). To confirm the presence of RBCs and evaluate whether the ECs were of human origin, tissue sections were immunohistochemically stained for Ter-119, an erythroid cell marker, and human-specific CD31 (Fig. 2*C*). Ter-119 staining confirmed the presence of RBCs at all time points in localized patterns matching those previously observed with H&E staining. Human ECs circumscribed the RBCs and were found at all stages of the process, suggesting the formation of blood vessels containing ECs of human origin. These vessels appeared large and poorly organized at days 3 and 5 PI, but rapidly remodeled into smaller, lumenized capillaries that were evident as early as 7 d PI and persisted until at least 28 d PI. Staining for alpha-smooth muscle actin (α-SMA) revealed the presence of α-SMA–positive cells in a perivascular localization as early as day 3 (Fig. 2*D*). As nascent vessels reorganized into smaller capillaries, the α-SMA–positive cells were tightly associated with adjacent ECs, suggesting a pericyte phenotype. To better assess the dynamics of vessel remodeling, we quantified the surface area of blood, the total number of vessels, and the diameter of vessels in H&E-stained sections (*SI Materials and Methods*). This quantification suggested that the maturation of capillaries occurred primarily between days 5 and 7 PI, during which (*i*) the area of blood within cords decreased from ∼65% to 25% of the total cord area, (*ii*) the number of capillaries per cord increased from ∼1.5 to 4.0, and (*iii*) the average vessel diameter decreased from ∼30 μm to 7 μm (Fig. 2*E*; $P < 0.05$). All trends continued until at least 28 d PI. Together, these results suggest that engineered cords anastomose quickly (by day 3 PI) with the host vasculature to form large, nascent vessels that later lumenize and reorganize into smaller, more numerous, and mature capillaries that are organized spatially around and alongside the collagen core of the endothelial cords.

The vascularization response appeared to be specific to the cords, as implanted acellular, control fibrin gels remained absent of cells and showed no evidence of blood at 7 d PI (Fig. S2*A*). To determine whether cells within the engineered cords were required only for the in vitro assembly of the cord matrix and not necessary during implantation to elicit the vascularization response, we implanted tissue constructs consisting of fibrin gels containing cords that had been "decellularized" via treatment with CHAPS detergent before implantation. These gels retained the matrix structure of the cords, but cells were removed. Analysis of decellularized cords post implantation indicated the presence of small nuclei or DNA fragments near areas of collagen matrix, but no blood was evident (Fig. S2*B*). Together, these studies indicate that living cells within the cords were required for the biological activity of the constructs.

To study the impact of cellular organization within the implant on the vascularization response, we generated and implanted fibrin gels containing randomly seeded HUVECs and 10T1/2s that had been precultured for 7 d in vitro. Gels resected 7 d PI suggested the formation of a small number of capillaries limited to the periphery of the constructs penetrating no more than several hundred microns toward the core (Fig. S2*C*). In contrast, cord-containing constructs exhibited the presence of blood and vessels throughout the length of the cords. Notably, optimized random controls required 2×10^6 cells per milliliter, more than an order of magnitude more cells per implant than the patterned cord implants. Together, these results demonstrate that viable endothelial and mural cells,

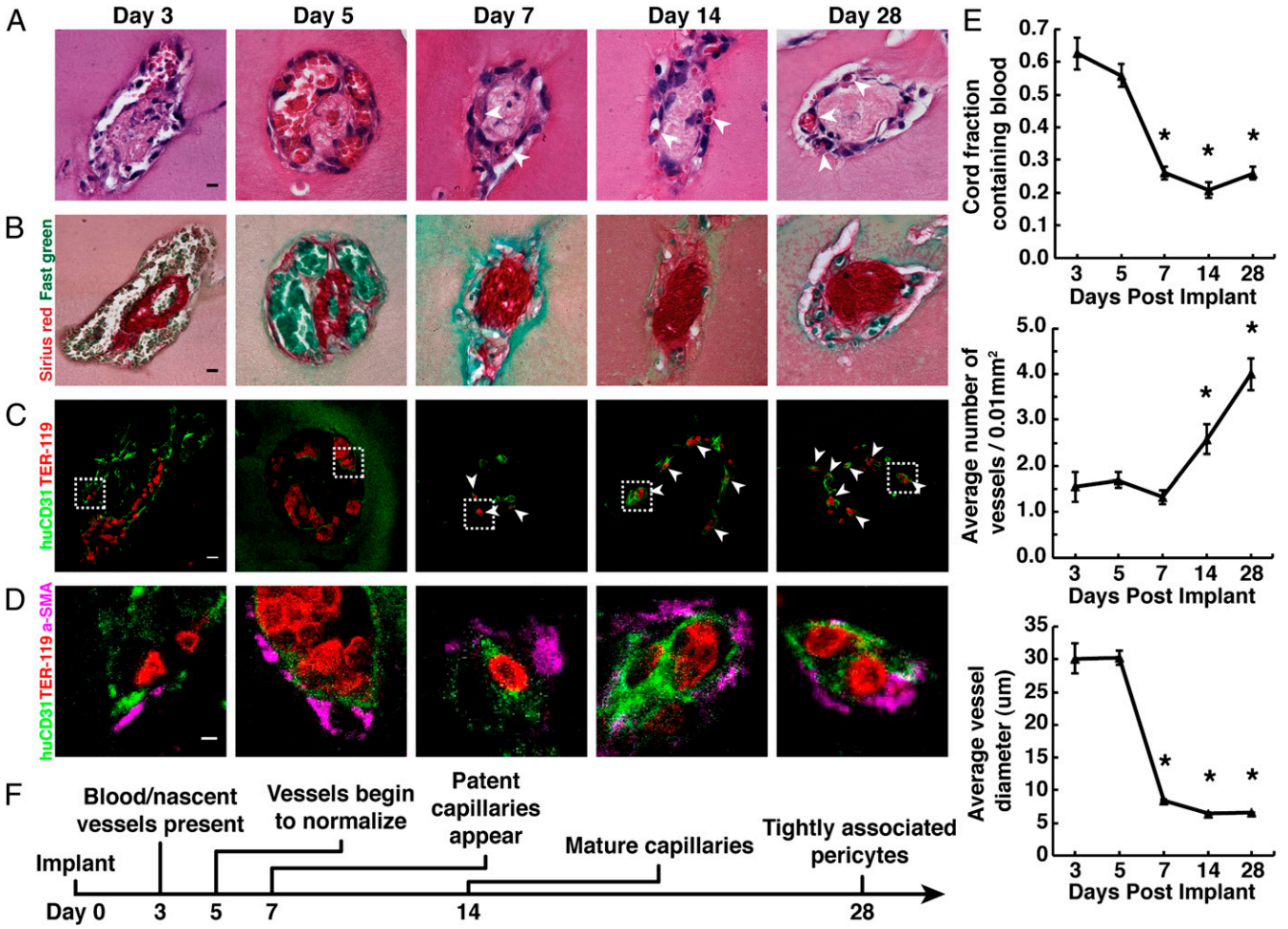

Fig. 2. Implanted EC cords drive formation of stable capillaries. (*A*) H&E staining of EC cords resected at days 3, 5, 7, 14, and 28 PI suggests the presence of blood within vessels that organize into small capillaries by day 7 (arrowheads) (bar, 10 μm). (*B*) Sirius red/fast-green staining of collagen within the cords after harvest (bar, 10 μm). (*C*) Ter-119 (red) and human-specific CD31 (green) staining positively identify RBCs and ECs and suggest that vessels were of human origin (bar, 10 μm). (*D*) α-SMA–positive (magenta) cells with a perivascular localization are seen at higher magnification (bar, 20 μm). (*E*) Quantification of blood area, vessel diameter, and vessel numbers over 28 d. $*P < 0.05$ for comparison of days 7, 14, and 28 vs. 3 and 5 in blood area and vessel diameter measurements, and days 14 and 28 vs. 3, 5, and 7 in vessel number measurements. Error bars: SEM, $n \geq 20$, one-way ANOVA followed by Tukey's post hoc test. (*F*) Timeline representation of vessel maturation.

as well as geometric definition of cord structure, contribute to the robust vessel formation and graft–host integration.

Geometrically Defined EC Cords in Vitro Yield to Patterned, Perfused Vessels in Vivo After Implantation. To observe more convincingly whether these newly formed capillaries lining the cords had functionally anastomosed with the host vasculature and were perfused, we performed injections of 150 kDa FITC-dextran via the tail vein at day 14 PI and then immediately imaged the implant site. FITC-dextran injections of control mice implanted with fibrin gels containing randomly seeded HUVECs and 10T1/2s resulted in random assembly of vessels exhibiting some degree of perfusion, but such perfusion was observed only near the periphery of implanted constructs (Fig. 3*A*, *Left*). Conversely, FITC-dextran injection of mice containing tissue constructs with cords demonstrated extensive perfusion of capillaries that spanned the entire length of the constructs. The dextran was contained exclusively within the intraluminal space of the neovessels, demonstrating that blood was not leaking into the interstitium. Importantly, we noted that the original network architecture of the cords visibly templated the new capillary vasculature. Constructs containing parallel arrays of cords resulted in a largely parallel capillary network, and introducing a single cord with a bifurcation resulted in a perfused branch point (Fig. 3*A*, *Center* and *Right*). For parallel cords, the resulting capillary network did not remain exclusively along the cords, as we observed occasional sprouts containing blood extending between adjacent parallel cords at day 14 (Fig. 3*A*, *Center*) and day 7 (Fig. S3) PI.

To determine the contribution of grafted and host ECs to the vascular interface of perfused capillaries, we injected mouse- and human-specific lectins [*Helix pomatia* agglutinin (HPA)–Alexa Fluor 488 and *Ulex europaeus* agglutinin I (UEA-I)–TRITC, respectively] via tail vein at day 14 PI and performed fluorescent imaging. Perfused microvascular networks in the graft area were composed of a parallel array of patent capillaries that appeared chimeric in composition (Fig. 3*B*). Stretches of capillaries that bound solely to UEA-1 or to HPA were visible throughout the constructs, suggesting that regions of perfused vessels were composed primarily of human or mouse ECs and confirmed previously reported species specificity of UEA-1 or HPA in our samples (18, 19). In addition, large stretches of capillaries colabeled with both lectins suggested chimeric composition of host and implanted cells in some vessels. Outside the boundary of the implant and cords, vessels were of mouse origin and individual vessels appeared to

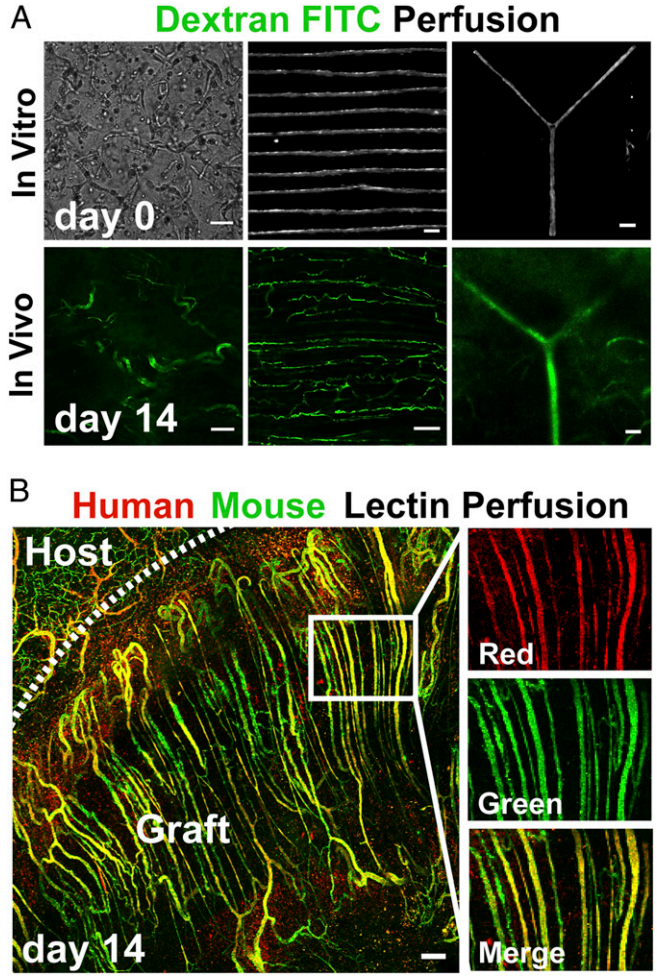

Fig. 3. Patterned EC cords integrate with host vasculature. (*A*) Bright field images of fibrin gels in vitro before implantation, which contain self-organized networks of HUVECs and 10T1/2s, patterned EC cords, or EC cords patterned into a branched topology (*Upper* row; bars: 250 μm, 500 μm, and 500 μm, respectively). (*Upper* row) These samples were implanted in the intraperitoneum of nude mice, and after 14 d FITC-dextran was perfused via tail vein injection. (*Lower* row) Representative FITC-dextran images (bars, 100 μm). (*B*) To further distinguish human from mouse endothelium, gels containing parallel arrays of cords were implanted, and mice were perfused with human-specific lectin (UEA-1–TRITC) and mouse-specific lectin (HPA–Alexa 488) via tail vein injection at 14 d PI. Representative images demonstrate that the resultant perfused microvascular network of the graft is composed of a parallel array of patent capillaries that are chimeric in composition (red, human; green, mouse; bar, 150 μm).

anastomose with multiple cord-associated capillaries. Imaging of host adipose tissue confirmed the lack of cross-reactivity between UEA-I and mouse vessels (Fig. S4). Further immunostaining using antibodies specific to mouse or human CD31 confirmed that both mouse and human ECs contributed extensively to capillaries in the graft (Fig. S5). Together, these results demonstrate that geometrically controlled engineered vessels are perfused after implantation and that implanted cords anastomose with host tissue via a mechanism that involves, at least in part, ingrowth of host vessels into tissue constructs and connection to regions of vessels lined with a chimeric mixture of both graft- and host-derived endothelium.

Spatially Patterned Endothelial Cords in Engineered Hepatic Tissues Improves Hepatocyte Function. We next sought to test whether geometrically controlled prevascularization of tissue constructs could affect parenchymal tissue survival and function (Fig. 4). Primary hepatocytes expressing luciferase under the control of a modified albumin promoter were aggregated into spheroids (Fig. 4*A*) to promote maintenance of their differentiated function (2, 20). To assess whether endothelial cords would support primary hepatocytes after implantation, tissue constructs containing rat hepatocyte aggregates and endothelial cords were sutured to the parametrial fat pad in athymic mice and were compared with control constructs containing rat hepatocyte aggregates only. Histological assessment of tissues explanted at day 20 revealed the presence of patterned collagen structures similar to those found in constructs with cords alone in earlier experiments (Fig. 4*B*, *Left*; black arrows). Collagen structures were closely associated with capillaries carrying fast-green–positive blood (Fig. 4*B*, white arrows) and cellular aggregates (Fig. 4*B*, dotted line). Immunofluorescent staining for RBCs and hepatocytes [Ter-119 and arginase 1 [ARG-1], respectively) suggested the presence of perfused neovessels directly adjacent to hepatocyte aggregates (Fig. 4*B*, *Right*). Hepatic tissues containing EC cords exhibited significantly greater albumin promoter activity for at least 20 d PI compared with tissues with no EC cords (Fig. 4*C*), suggesting a direct benefit from the cords.

To explore whether this vascularization strategy has potential to enable applications such as human tissue replacement or humanized mouse models, we tested whether coimplantation of EC cords could support primary human hepatocytes. Similar to constructs with rat hepatocytes and EC cords, constructs with human hepatocytes and EC cords exhibited Sirius red-positive collagen cores in graft areas (Fig. 4*D*, *Left*; black arrows). Further staining with both Sirius red and fast green suggested the presence of capillaries containing blood (white arrows) as well as cellular aggregates (dotted line) adjacent to collagen-rich cores (Fig. 4*D*, *Center*; black arrows). Importantly, triple immunostaining demonstrated that capillaries in the graft were lined with human endothelium (huCD31, red), contained erythrocytes (Ter-119, white), and were close to aggregates containing hepatocytes (ARG-1, green) (Fig. 4*D*, *Right*). Tissue constructs containing human hepatocyte aggregates and EC cords ("EC Cord") exhibited significantly higher levels of albumin promoter activity compared with both constructs without cords ("No EC") and constructs with randomly seeded endothelial and 10T1/2 cells ("Random EC"; Fig. 4*E*). To test whether enhanced hepatic function in animals with EC cords was the result of direct paracrine signaling between adjacent EC cords and hepatocytes or of improved access to a blood supply, we severed the parametrial fat pad upstream of our constructs immediately after implantation to reduce blood supply ("EC Cord Ligated"; Fig. 4*E*). Bioluminescence imaging was performed 20 min after luciferin injection at each time point, which we confirmed to be adequate time for diffusion-based permeation of the construct in ligated control tissues by DAPI (a small molecule similar in size to luciferin; Fig. S6). Poor functional performance of ligated control constructs suggested that enhanced hepatocyte activity in the presence of EC cords was a result of improved access to blood-carrying vasculature (Fig. 4*E*). Taken together, these results show that geometric control of endothelial and mural cells during prevascularization of tissue constructs enhances vascular blood supply and improves survival and function of human hepatic tissue.

Discussion

Several recent studies have shown that combining randomly distributed ECs with supportive stromal cells provides a means to induce the formation of stable vasculature in a tissue engineered implant (3, 9, 13, 15, 16, 21). Allowing these cells to form interconnected networks in culture before implantation (prevascularization) appears to improve the rapidity and extent of the vascularization response (1, 4, 5, 10). Here, we introduce the concept of prepatterning the cells using microfabrication

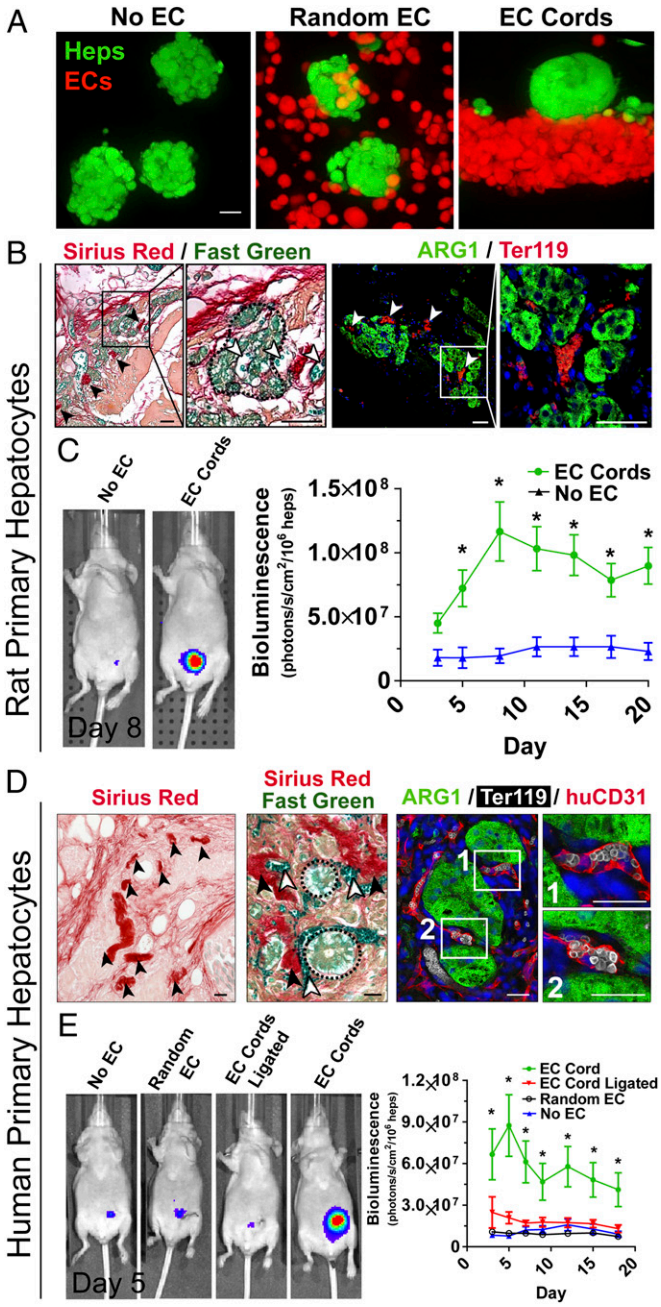

Fig. 4. EC cords within engineered hepatic tissue improve function. (*A*) Three types of tissue constructs were generated: (*i*) hepatocyte aggregates only (No EC), (*ii*) randomly seeded HUVECs and 10T1/2s with hepatocyte aggregates (Random EC), and (*iii*) hepatocyte aggregates adjacent to EC cords (EC Cord; bar, 20 μm) using labeled hepatocytes (green, calcein AM) and HUVECs (calcein, red-orange). (*B*) Sirius red/fast-green staining (*Left*) revealed cellular aggregates (dotted line) close to spatially patterned collagen structures (black arrows) indicative of cords as well as to vessels that appeared to carry fast-green–stained blood (white arrows; bar, 50 μm). Immunostaining for Ter-119 (red; erythrocytes) and ARG-1 (green; hepatocytes) confirmed the presence of RBCs directly adjacent to viable hepatocyte aggregates at 20 d PI (*Right* bars, 25 μm). (*C*) Luciferase activity showed significantly increased albumin promoter activity in the tissue constructs containing patterned rat hepatocyte aggregates and EC cords at least 20 d PI. Error bars: SEM, $n = 13$ and 5 for EC Cords and No EC groups, respectively. $^*P < 0.05$, one-way ANOVA followed by Tukey's post hoc test. (*D*) Similar to histochemistry for rat hepatic tissues, Sirius red staining demonstrated the presence of patterned collagen remnants of cords (*Left*). Further addition of fast green identified capillaries containing blood (white arrows) as well as cellular aggregates (dotted line) near these collagen cores (*Center*). Triple immunostaining for ARG-1 (green; hepatocytes), Ter-119 (white; erythrocytes), and huCD31 (red; human endothelial cells) demonstrated localization of RBCs within capillaries that were lined with human endothelium and immediately adjacent to viable hepatocyte aggregates (*Right*; bars, 25 μm). (*E*) Representative images of luciferase activity under the control of the albumin promoter show increased primary human hepatocyte function in constructs containing patterned EC cords. Constructs containing human hepatocytes patterned with EC cords performed significantly better than all control groups for at least 18 d PI. Albumin promoter activity was similar among control groups, which contained EC cords but were ligated upon implantation (EC Cord Ligated), randomly seeded HUVECs and 10T1/2s (Random EC), or no cells (No EC). Error bars: SEM, $n = 11$, 7, 5, and 6 for EC Cord, No EC, EC Cord Ligated, and Random EC groups, respectively. $^*P < 0.05$, one-way ANOVA followed by Tukey's post hoc test.

approaches, which allows for the formation of reproducible, multicellular cords within hours. In contrast, culture of randomly distributed cells is typified by nonuniform rate, length, diameter, and orientation of tubule formation, and the resultant microvascular networks exhibit tortuous morphology and dense interconnectivity after implantation. Here, implantation of endothelial cords led to rapid anastomosis with the host vasculature (within 3 d), followed by the formation of large, nascent vessels that later reorganized into smaller, more numerous capillaries composed, at least in part, of implanted ECs. In our studies, viable cells within cords were required for and contributed directly to the vascularization response. These results correspond with previous studies in which randomly distributed cells within implanted constructs contributed directly to the formation of vessels (2, 6, 9, 21). Additionally, studies have shown that implanted ECs anastomose by migrating toward and tapping into existing host vasculature (3, 7, 8, 22). Capillaries within implanted cords, however, seemed to exhibit a chimeric phenotype, suggesting that directed angiogenic sprouting of the host vasculature occurred during anastomosis. The vascularization response observed upon implantation of EC cords likely is driven by a mechanism involving both angiogenesis, which promotes sprouting from the host vasculature, and vasculogenesis, which promotes the assembly of capillaries from implanted cells.

Patterning vascular architecture remains a key challenge in engineering complex, metabolically active tissues such as kidney and liver (9–12, 23). Previously, physical and biochemical means have been used to spatially guide the host angiogenic response in tissue engineered constructs (12–16, 24, 25). Although these approaches rely on the relatively slow ingrowth of vessels from host tissue, the implanted EC cords introduced here appear to act as a guide for a rapid vascularization response that results in nearly complete and templated perfusion of all cords throughout the construct. Importantly, the parallel capillary network formed in our studies is highly organized compared with the networks created by prevascularization via random cell seeding and self-organization, which are characterized by tortuous morphology and dense interconnectivity. Indeed, a recent study demonstrated that although such randomly organized networks initially connect rapidly to host vessels, perfusion is lost after 5 d by thrombus formation secondary to low shear rates in these highly irregular networks (26). This finding is in sharp contrast to the response of our architectural arrays of largely parallel capillaries, which remain patent and perfused at least 2 wk after implantation. Together, these results suggest that the caliber, tortuosity, and interconnectivity of the endothelial networks may play a major role in the vascularization process. This hypothesis is supported by mathematical models, in which the architecture of mature capillary beds has been predicted to affect blood flow and nutrient delivery (27, 28). The ability to control vascular architecture using methods demonstrated here will enable studies of the effects of vascular features such as vessel density, alignment, and branching on tissue oxygenation and function and will inform the generation of custom tissue-specific vascular architectures.

Intricate interactions among hepatocytes, ECs, and other nonparenchymal cell populations are critical for efficient macromolecular and drug transport as well as response to regenerative cues in the liver. For example, hypoxic hepatocytes express angiogenic factors that recruit ECs (and other nonparenchymal cells) in liver injury and repair, and liver sinusoidal ECs secrete "angiocrine" signals that mediate liver regeneration (29, 30). Furthermore, the 3D spatial arrangement of these cells is tightly regulated in development, has been suggested to at least partially coordinate regeneration, and is dysfunctional in pathological states such as cirrhosis (31). Although models have been developed to "prevascularize" engineered hepatic and hepatoma tissue using ECs in vitro (32, 33), the fate of prevascularized constructs after in vivo implantation had not been documented before our study. Here, we demonstrate that implantation of engineered tissue containing primary hepatocytes and geometrically defined endothelial cords stabilized by stromal cells augments hepatic albumin activity following transplantation. Importantly, vessel organization and perfusion with blood were both critical to functional benefit, as this effect was not seen in constructs containing randomly seeded ECs or with cords lacking a blood supply. Thus, by improving tissue perfusion through the geometric control over implanted cells, this work provides a strategy to enable improved tissue integration function due to enhanced blood supply.

Materials and Methods

EC cords were micropatterned as previously described (17). HUVECs and 10T1/2s were suspended at a ratio of 50:1 in 2.5 mg/mL liquid collagen (BD Biosciences) and centrifuged into PDMS channels pretreated with 0.01% Pluronic F-127. Excess unpolymerized collagen and cells were removed by dewetting the surface of the substrate. The collagen was polymerized, growth medium was added, and constructs were incubated for 4–6 h. The newly formed cords were removed from the PDMS substrates by inverting onto a drop of unpolymerized 7.5 mg/mL bovine fibrin (Sigma–Aldrich). After the fibrin was polymerized, the PDMS was removed, and a second layer of unpolymerized fibrin was added and polymerized to fully encase the cords. The embedded cords were cut with a 6-mm biopsy punch before implantation. To include hepatocytes in the constructs, hepatic aggregates comprising ~100 hepatocytes and 25 J2 fibroblasts were formed in AggreWell micromodels overnight and suspended at a concentration of 15K/mL in the fibrin gel. Random HUVEC conditions included 2×10^6 HUVECs per milliliter and 10T1/2s at a 50:1 ratio in fibrin. For decellularization, constructs were immersed in 8 mM CHAPS, 1 M NaCl, and 25 mM EDTA in PBS and placed on an orbital shaker overnight. Excess cellular debris and detergent were then removed by soaking the constructs multiple times in PBS on an orbital shaker for several hours. For more details, please see *SI Materials and Methods*.

ACKNOWLEDGMENTS. We thank C. Choi, M. Wozniak, H. Fleming, and E. Vasile for helpful discussions, the P. Zandstra laboratory for AggreWell micromolds, and Charles Rice for lentivirus. This work was supported by National Institutes of Health (NIH) Grants EB08396 and EB00262. Individual fellowship support was provided by NIH National Research Service Award 1F32DK091007 (to K.R.S.) and 5T32AR007132-35 (to R.R.C.). S.N.B. is a Howard Hughes Investigator.

1. Vacanti JP, Langer R (1999) Tissue engineering: The design and fabrication of living replacement devices for surgical reconstruction and transplantation. *Lancet* 354(Suppl 1):SI32–SI34.
2. Lovett M, Lee K, Edwards A, Kaplan DL (2009) Vascularization strategies for tissue engineering. *Tissue Eng Part B Rev* 15(3):353–370.
3. Jain RK (1999) Transport of molecules, particles, and cells in solid tumors. *Annu Rev Biomed Eng* 1:241–263.
4. Folkman J (2002) Looking for a good endothelial address. *Cancer Cell* 1(2):113–115.
5. Radisic M, et al. (2003) High-density seeding of myocyte cells for cardiac tissue engineering. *Biotechnol Bioeng* 82(4):403–414.
6. Reid LM, Fiorino AS, Sigal SH, Brill S, Holst PA (1992) Extracellular matrix gradients in the space of Disse: Relevance to liver biology. *Hepatology* 15(6):1198–1203.
7. Richardson TP, Peters MC, Ennett AB, Mooney DJ (2001) Polymeric system for dual growth factor delivery. *Nat Biotechnol* 19(11):1029–1034.
8. Lee KY, Peters MC, Anderson KW, Mooney DJ (2000) Controlled growth factor release from synthetic extracellular matrices. *Nature* 408(6815):998–1000.
9. Koike N, et al. (2004) Tissue engineering: Creation of long-lasting blood vessels. *Nature* 428(6979):138–139.
10. Chen X, et al. (2009) Prevascularization of a fibrin-based tissue construct accelerates the formation of functional anastomosis with host vasculature. *Tissue Eng Part A* 15(6):1363–1371.
11. Melero-Martin JM, et al. (2008) Engineering robust and functional vascular networks in vivo with human adult and cord blood-derived progenitor cells. *Circ Res* 103(2): 194–202.
12. Kang K-T, Allen P, Bischoff J (2011) Bioengineered human vascular networks transplanted into secondary mice reconnect with the host vasculature and re-establish perfusion. *Blood* 118(25):6718–6721.
13. Levenberg S, et al. (2005) Engineering vascularized skeletal muscle tissue. *Nat Biotechnol* 23(7):879–884.
14. Kaufman-Francis K, Koffler J, Weinberg N, Dor Y, Levenberg S (2012) Engineered vascular beds provide key signals to pancreatic hormone-producing cells. *PLoS One* 7(7):e40741.
15. Koffler J, et al. (2011) Improved vascular organization enhances functional integration of engineered skeletal muscle grafts. *Proc Natl Acad Sci USA* 108(36): 14789–14794.
16. Stevens KR, et al. (2009) Physiological function and transplantation of scaffold-free and vascularized human cardiac muscle tissue. *Proc Natl Acad Sci USA* 106 (39):16568–16573.
17. Raghavan S, Nelson CM, Baranski JD, Lim E, Chen CS (2010) Geometrically controlled endothelial tubulogenesis in micropatterned gels. *Tissue Eng Part A* 16(7):2255–2263.
18. Debbage PL, et al. (2001) Intravital lectin perfusion analysis of vascular permeability in human micro- and macro- blood vessels. *Histochem Cell Biol* 116(4):349–359.
19. Debbage PL, et al. (1998) Lectin intravital perfusion studies in tumor-bearing mice: Micrometer-resolution, wide-area mapping of microvascular labeling, distinguishing efficiently and inefficiently perfused microregions in the tumor. *J Histochem Cytochem* 46(5):627–639.
20. Brophy CM, et al. (2009) Rat hepatocyte spheroids formed by rocked technique maintain differentiated hepatocyte gene expression and function. *Hepatology* 49(2): 578–586.
21. Chen X, et al. (2010) Rapid anastomosis of endothelial progenitor cell-derived vessels with host vasculature is promoted by a high density of cotransplanted fibroblasts. *Tissue Eng Part A* 16(2):585–594.
22. Cheng G, et al. (2011) Engineered blood vessel networks connect to host vasculature via wrapping-and-tapping anastomosis. *Blood* 118(17):4740–4749.
23. Vacanti JP (2012) Tissue engineering and the road to whole organs. *Br J Surg* 99(4): 451–453.
24. Chen RR, Silva EA, Yuen WW, Mooney DJ (2007) Spatio-temporal VEGF and PDGF delivery patterns blood vessel formation and maturation. *Pharm Res* 24(2):258–264.
25. Jeong JH, et al. (2012) "Living" microvascular stamp for patterning of functional neovessels; orchestrated control of matrix property and geometry. *Adv Mater (Deerfield Beach Fla)* 24(1):58–63, 1.
26. White SM, et al. (2012) Longitudinal in vivo imaging to assess blood flow and oxygenation in implantable engineered tissues. *Tissue Eng Part C Methods* 18(9):697–709.
27. Intaglietta M, Johnson PC, Winslow RM (1996) Microvascular and tissue oxygen distribution. *Cardiovasc Res* 32(4):632–643.
28. Pittman RN (1995) Influence of microvascular architecture on oxygen exchange in skeletal muscle. *Microcirculation* 2(1):1–18.
29. Rosmorduc O, Housset C (2010) Hypoxia: A link between fibrogenesis, angiogenesis, and carcinogenesis in liver disease. *Semin Liver Dis* 30(3):258–270.
30. Ding B-S, et al. (2010) Inductive angiocrine signals from sinusoidal endothelium are required for liver regeneration. *Nature* 468(7321):310–315.
31. Matsumoto K, Yoshitomi H, Rossant J, Zaret KS (2001) Liver organogenesis promoted by endothelial cells prior to vascular function. *Science* 294(5542):559–563.
32. McGuigan AP, Sefton MV (2006) Vascularized organoid engineered by modular assembly enables blood perfusion. *Proc Natl Acad Sci USA* 103(31):11461–11466.
33. Nahmias Y, Berthiaume F, Yarmush ML (2007) Integration of technologies for hepatic tissue engineering. *Adv Biochem Eng Biotechnol* 103:309–329.

Supporting Information

Baranski et al. 10.1073/pnas.1217796110

SI Materials and Methods

Cell Culture. Primary human umbilical endothelial cells (HUVECs; Lonza) were maintained on 0.1% (wt/vol) gelatin-coated dishes in EGM-2 (Lonza). C3H10T1/2 cells (ATCC) were maintained in low-glucose DMEM containing 10% (vol/vol) FBS (Atlanta Biologicals), 100 U/mL penicillin, and 100 mg/mL streptomycin (Invitrogen). Primary human hepatocytes from a 1-y-old female Caucasian donor (Lot Hu8085; CellzDirect) were maintained in high-glucose DMEM (Cellgro) containing 10% (vol/vol) FBS (Gibco), 1% (vol/vol) ITS (insulin, transferrin, sodium selenite) supplement (BD Biosciences), 0.49 pg/mL glucagon, 0.08 ng/mL dexamethasone, 0.018 M Hepes, and 1% (vol/vol) penicillin–streptomycin (pen-strep; Invitrogen). Primary rat hepatocytes were isolated as described previously (1–4) and maintained in high-glucose DMEM containing 10% (vol/vol) FBS, 0.5 U/mL insulin (Lilly), 7 ng/mL glucagon (Bedford Laboratories), 7.5 μg/mL hydrocortisone (Sigma–Aldrich), and 1% (wt/vol) pen-strep. J2-3T3 fibroblasts (gift from Howard Green, Harvard Medical School, Boston) were maintained in high-glucose DMEM containing 10% (vol/vol) bovine serum and 1% (wt/vol) pen-strep. Human hepatoma (Huh-7.5) cells (gift from Charles Rice, The Rockefeller University, New York) were maintained in high-glucose DMEM containing 10% (vol/vol) FBS (Atlanta Biologicals), 100 U/mL penicillin, and 100 mg/mL streptomycin (Invitrogen) and used for in vitro imaging of hepatic constructs instead of primary hepatocytes.

In Vivo Implantation of Constructs. All surgical procedures were conducted according to protocols approved by the University of Pennsylvania or Massachusetts Institute of Technology Institutional Animal Care and Use Committee. To preserve geometry during implantation, constructs were embedded in a gasket cut from a polypropylene surgical mesh (Davol). Eight-week-old female Nu/nu nude mice (Charles River) or NCr nude mice (Taconic) were anesthetized using isoflurane, and the constructs were sutured to the mesenteric parametrial fat pad. For "cords + hepatocytes – excised" animals, engineered tissue and attached mesentery were cut from the remainder of the mesentery via an upstream excision so that the tissue and attached mesentery were isolated from host circulation. The incisions were closed aseptically, and the animals were administered 0.1 mg/mL buprenorphine every 12 h for 3 d following surgery.

In Situ Imaging. To enable noninvasive imaging of function, hepatocytes were transduced with a lentiviral vector expressing firefly luciferase under the human albumin promoter (pTRIP.Alb.IVSb.IRES.tagRFP-DEST; gift of Charles Rice, The Rockefeller University, New York). For luminescence imaging, mice were injected i.p. with 250 μL of 15 mg/mL D-luciferin (Caliper Life Sciences) and then imaged using the IVIS Spectrum system (Xenogen). To visualize perfused vessels, a solution of 20 mg/mL FITC-labeled dextran (150 kDa; Sigma) in PBS was injected i.v. via the tail vein. To visualize mouse vs. human vessels, a solution of 500 μg/mL lectin from *Helix pomatia* agglutinin (HPA) conjugated to Alexa 488 (Sigma–Aldrich), and 100 μg/mL lectin from *Ulex europaeus* agglutinin (UEA-1) conjugated to TRITC (Vector Laboratories) in PBS was injected i.v. via the tail vein. These lectins previously were demonstrated to bind specifically to mouse or human endothelial cells, respectively (5, 6). Perfused vessels subsequently were imaged using a Zeiss 710 laser scanning confocal microscope.

Tissue Harvesting, Processing, and Histology, and Immunohistochemistry. Animals were killed at various time points, and tissue was harvested from the i.p. space. Explants were fixed in 4% (vol/vol) paraformaldehyde (PFA) for 48 h at 4 °C, dehydrated in graded ethanol (50–100%), embedded in paraffin, and sectioned using a microtome (6 μm) for immunohistochemical staining. For gross visualization of tissue, sections were stained with hematoxylin and eosin (H&E). For identification of cords composed partially of collagen, sections were stained with Sirius red (collagen) and fast green (other tissue elements). For identification of vessels containing human endothelial cells, mouse endothelial cells, smooth muscle cells, and erythroid cells, sections first were blocked using M.O.M. Blocking Reagent (Vector Laboratories) and normal goat serum and then immunostained using primary antibodies against human CD31 (1:20; Dako), mouse CD31 (1:50; BD Biosciences), Ter-119 (1:100; BD Biosciences), and alpha-smooth muscle actin (1:100, Abcam), respectively. Signal was visualized after incubation with secondary goat anti-IgG1–Alexa 555, goat anti-rat–Alexa 488, and donkey anti-rabbit–Alexa 647 antibodies (Jackson ImmunoResearch). For identification of primary hepatocytes adjacent to vessels containing RBCs, sections were blocked using normal donkey serum then incubated with primary antibodies against arginase 1 (ARG-1, 1:400; Sigma–Aldrich) and Ter-119 and followed with species-appropriate secondary antibodies conjugated to Alexa 488 and 555. Images were obtained using a Zeiss 710 laser scanning confocal or Nikon 1AR Ultra-Fast Spectral Scanning confocal microscope.

Statistical Analysis and Quantification of Vascularization Parameters. Quantification was performed manually on imaged H&E sections using FIJI Open Source software. Blood area was quantified by measuring the total area of tissue containing blood within a cord. Measurements were normalized to average cord area to compensate for oblique cutting angles. Vessel number was quantified by counting individual vessels within a cord and then normalized to the average cord area. Vessel diameter was quantified by measuring the diameter of individual vessels within a cord. Sections for quantification were chosen from the center of the constructs, and a minimum of three sections at least 150 μm apart were quantified per cord. All data are expressed as the mean ± SE. Statistical significance was determined using a one-way ANOVA followed by Tukey's post hoc test for group comparisons.

1. March S, Hui EE, Underhill GH, Khetani S, Bhatia SN (2009) Microenvironmental regulation of the sinusoidal endothelial cell phenotype in vitro. *Hepatology* 50(3): 920–928.
2. Chen AA, et al. (2011) Humanized mice with ectopic artificial liver tissues. *Proc Natl Acad Sci USA* 108(29):11842–11847.
3. Seglen PO (1976) Preparation of isolated rat liver cells. *Methods Cell Biol* 13:29–83.
4. Dunn JC, Tompkins RG, Yarmush ML (1991) Long-term in vitro function of adult hepatocytes in a collagen sandwich configuration.. *Biotechnol Prog* 7(3):237–245.
5. Debbage PL, et al. (2001) Intravital lectin perfusion analysis of vascular permeability in human micro- and macro- blood vessels. *Histochem Cell Biol* 116(4):349–359.
6. Debbage PL, et al. (1998) Lectin intravital perfusion studies in tumor-bearing mice: Micrometer-resolution, wide-area mapping of microvascular labeling, distinguishing efficiently and inefficiently perfused microregions in the tumor. *J Histochem Cytochem* 46(5):627–639.

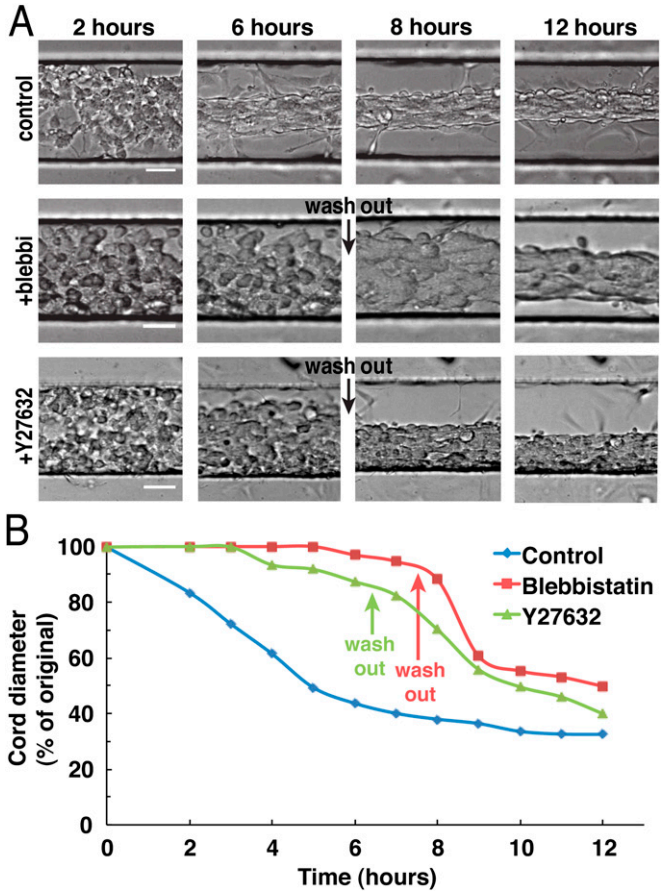

Fig. S1. Cytoskeletal tension is required for cord contraction. (*A*) Time-lapse imaging depicting cord formation in samples treated with vehicle, blebbistatin, or Y27632 (bar, 50 μm). (*B*) Quantification of cord contraction reveals rapid increase in contraction after wash-out of contractility inhibitors. Constructs were treated with 20 μM blebbistatin or 25 μM Y27632 at 7.5 or 6.5 h.

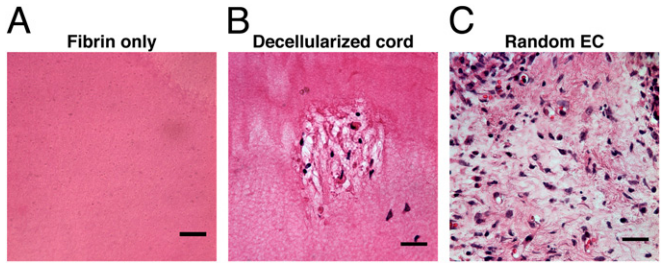

Fig. S2. Cells are required for vascularization. (*A*) H&E staining of fibrin gel (no cells) implanted and resected 5 d PI. (*B*) H&E staining of fibrin gel containing decellularized endothelial cell (EC) cords 5 d PI (bars, 25 μm). (*C*) Fibrin gel containing a mixture of HUVECs and 10T1/2s used in making EC cords. Cells were allowed to organize into networks in vitro for 2 d before implantation and resected 5 d PI.

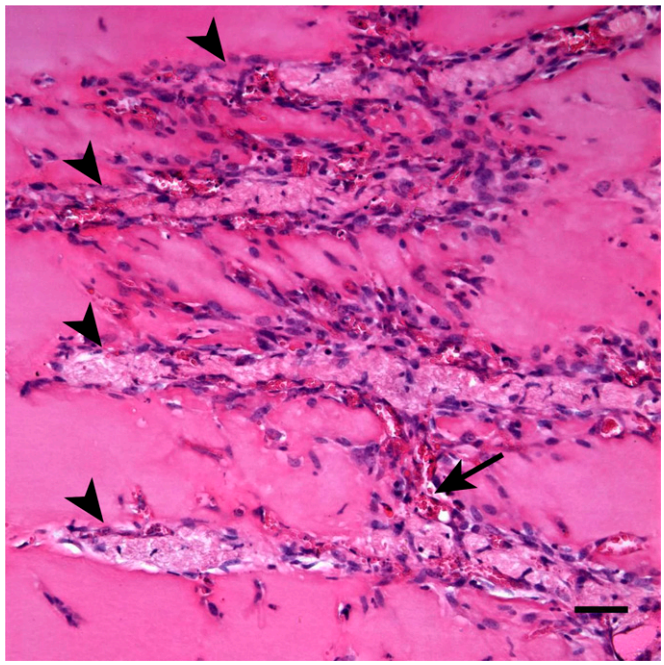

Fig. S3. Evidence of sprouting between capillaries within adjacent cords. H&E staining of longitudinal cord cross-sections at day 7 PI revealed evidence of capillary sprouts (arrow) between adjacent cords (arrowheads) (bar, 25 μm).

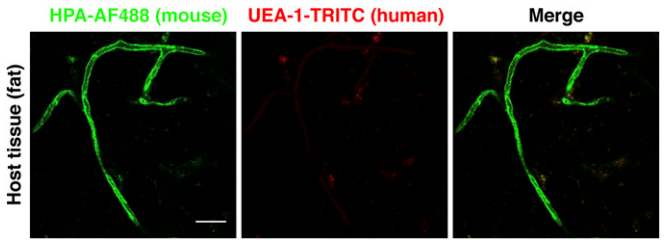

Fig. S4. Mouse and human lectin cross-reactivity. Human-specific (UEA-1) lectin and mouse-specific (HPA) lectin were perfused at 14 d following implantation of constructs. Imaging of surrounding host adipose tissue demonstrated minimal cross-reactivity between UEA-1 and mouse vessels (bar, 25 μm).

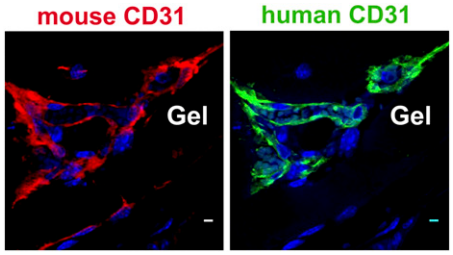

Fig. S5. Contribution of mouse vs. human endothelial cells to capillaries. Adjacent tissue sections were immunostained using antibodies specific for either mouse (*Left*) or human (*Right*) CD31. Capillaries in the grafts contained both human and mouse endothelium at 14 d PI (bar, 10 μm).

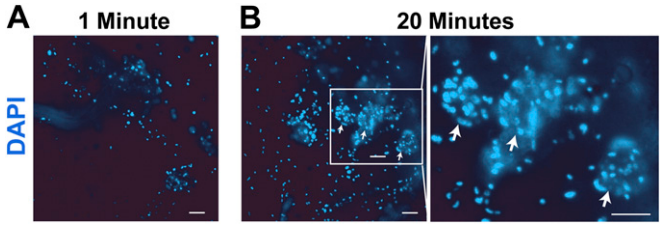

Fig. S6. Diffusion of small-molecule DAPI through ligated constructs. Constructs containing both hepatic aggregates and cords were implanted using procedures identical to those of the "EC Cord Ligated" control. Following implantation, the animals were injected i.p. with DAPI using the same volume and concentration typically used for luciferin administration. (*A*) Single dispersed DAPI-positive cells could be identified in constructs as early as 1 min after DAPI injection. (*B*) By 20 min post injection, DAPI-positive hepatic aggregates were identified throughout the constructs. These studies demonstrate that a small molecule similar in size to luciferin permeates the construct and stains hepatic aggregates within 20 min post injection within time scales relevant for bioluminescence imaging (bar, 50 μm).